

## The influence of load pulse shape on pressure-impulse diagrams of one-way RC slabs

Wei Wang<sup>a</sup>, Duo Zhang and Fangyun Lu\*

*Institute of Technique Physics, College of Science, National University of Defense Technology, Changsha, Hunan, 410073, P.R. China*

*(Received February 16, 2011, Revised March 24, 2012, Accepted April 2, 2012)*

**Abstract.** This study is aimed at providing an efficient analytical model to obtain pressure-impulse diagram of one-way reinforced concrete slabs subjected to different shapes of air blast loading using single degree of freedom method (SDOF). A tri-linear elastic perfectly plastic SDOF model has been used to obtain the pressure-impulse diagram to correlate the blast pressure and the corresponding concrete flexural damage. In order to capture the response history for the slab, a new approximately SDOF method based on the conventional SDOF method is proposed and validated using published test data. The influences of pulse loading shape on the pressure-impulse diagram are studied. Based on the results, a pressure-impulse diagram generation method using SDOF and an analytical equation for the pressure-impulse diagram is proposed to different damage levels and different blast loading shapes.

**Keywords:** blast load; SDOF; pressure-impulse diagram; one-way concrete slab

---

### 1. Introduction

In World War II, pressure-impulse (P-I) diagram method was first used to assess damage of structural elements and buildings. The assessment of damage can be carried out by defining a series of pressure impulse combinations to specific structures or structural elements. The early application of P-I diagrams was based on empirically derived diagrams for brick houses to determine damage criteria for other houses, small office buildings, and light-framed industrial buildings (Baker *et al.* 1983). P-I diagrams were also developed to assess human response to blast loading and to establish damage criteria for specific organs (e.g., eardrum, lungs, etc.) of the human body. In protective design, P-I diagrams have been extensively used for approximate damage assessments of structural components when subjected to blast loading.

P-I diagrams are applicable to any type of non-periodic dynamic load with a finite duration. The structure or structural component subjected to blast loading should have an unambiguous damage criterion. However, it is possible to combine P-I diagrams for different failure modes (e.g., shear and bending failure), as shown by Ma *et al.* (2007). Text books such as text books edited by Smith and Hetherington (1994) and by Kappos (2002) featuring P-I diagrams are often based on

---

\*Corresponding author, Ph.D. Candidate, E-mail: [fangyunlu@126.com](mailto:fangyunlu@126.com)

<sup>a</sup>E-mail: [wangwei591@gmail.com](mailto:wangwei591@gmail.com)

equivalent single degree of freedom (SDOF) systems. P-I diagrams based on SDOF systems are directly linked to the dynamic load factor (DLF). Both the derivation of the DLF and the equivalent SDOF systems can be found in Biggs (1964). A SDOF model is based on an assumption that the dynamic response of the structure or structural component is mainly determined by a single, dominant response mode. P-I diagrams for SDOF systems depend on the natural frequency of the system, the defined damage criterion, the pulse shape, the material behavior and the resistance function of the structure.

Symonds (1953) found that the final deflection of a free beam, when subjected to a concentrated pulse load, depends only on the total impulse  $I$  and peak load  $P_{max}$  of the pulse within a discrepancy of about 15%. However, his conclusion is valid only for loading intensities far beyond the yield load. The difference of the pulse loading shape has a profound influence on the dynamic response of structures and P-I diagrams of structure components. Studies on this topic have been conducted for various metallic structural members, such as, beams, plates, and shells, within the category of dynamic plastic response (Youngdahl 1970, Zhu *et al.* 1986, Li and Shu 1992, Li and Jones 1994, Li and Jones 1995a, b, Li and Jones 2001). However, this issue has not attracted enough attention for researchers and designers in civil engineering.

A great progress on developing P-I diagrams of structure components has been made in the recent years. Li and Meng (2002a, b) have studied the influence of the pulse shape on the P-I diagram for a linear-elastic SDOF system and an elastic-plastic SDOF system. Fallah and Louca (2007) also have derived P-I diagram from analyzing SDOF with elastic-plastic hardening and elastic-plastic softening under blast load. Most investigations only consider an idealized blast load, which is decaying with a maximum pressure at beginning. For these types of the pulse shape, the SDOF P-I diagram is of a hyperbolic shape. The pulse shapes with finite rise time result in P-I diagrams that are not of a hyperbolic shape, as shown in Smith and Hetherington (1994). When the material behavior and the pulse shape become too complex for an analytical solution, P-I diagrams can be derived numerically, as described by Krauthammer *et al.* (2008). It can be concluded that P-I diagrams are generally derived from equivalent SDOF systems, which are deduced from structural components (or structures). Recently a few researchers have also reported their attempt to use the pressure-impulse diagrams to evaluate damage levels of various structural members (Lan and Crawford 2003, Wesevich and Oswald 2005, Shi *et al.* 2008, Park and Krauthammer 2009).

However, the pressure-impulse diagrams generated by the current approaches may not give reliable prediction of structure component damage because of the following reasons: the SDOF analysis is incapable of capturing a spatially distribution and temporally varying of blast loading, can not allow for variations of mechanical properties of the cross-section along the member, cannot simultaneously accommodate shear and flexural deformations, and can only address strain rate effects indirectly, and may result in very conservative answers. And most pressure-impulse diagrams are based on the dimensionless force and impulse, and there is no efficient equation of pressure-impulse curves especially for reinforced concrete structures with different load shapes.

The object of the present work is to generate a pressure-impulse diagram for reinforced concrete slab for assessing blast damage more accurately by using the SDOF model. The SDOF method with simplified tri-linear resistance function, and we have considered a new method of capturing a spatially distribution and temporally varying of blast loading such as close-in explosion and it was validated with the experiments. The method is based on the damage criterion of rotation angel of the slab and based on the method the blast load shape effects on pressure-impulse diagram is investigated. In Section 2, we introduce the equivalent SDOF method using a reinforced concrete

beam as an example. Characteristics of pressure-impulse diagram are discussed in Section 3. A test result is compared to the analytical result to assess the effectiveness of SDOF method and P-I diagrams in blast damage assessment in Section 4. By using deformation based damage criterion, the pulse loading shape effects are discussed and their influence on the P-I diagrams according to different damage level are studied in Section 5. Based on the results, an analytical equation for the pressure-impulse diagram and a pressure-impulse diagram generation method using SDOF are proposed to different damage level and different blast loading shapes. It is shown that the proposed method gives a good prediction of pressure impulse diagrams of RC slabs and can be used for quick blast damage assessment.

## 2. Equivalent SDOF Method under blast loading

Single degree of freedom (SDOF) models have been widely used for predicting dynamic response of concrete structures subjected to blast and impact loading (Bangash 1993, Mays and Smith 1995). The popularity of the SDOF method in blast-resistant design lies in its simplicity and cost-effective approach that requires limited input data and less computational effort. Response of a SDOF structural model provides fundamental response mode, which is normally responsible for overall structural failure. This is illustrated in Fig. 1. With effective factors, such SDOF system can give out maximum displacement, velocity and acceleration quickly. Consequently damage assessment can be carried out based on the maximum displacement of the structure or elements.

As shown in Protective design manuals (TM 5-855-1 1986, TM 5-1300 1990, PDC-TR 06-01 Rev 1 2008), before analyzing the response of a structural element with distributed mass and loading, the mass, resistance and loading in Newton’s equation of motion are replaced with the equivalent values for a lumped mass-spring system in the Equivalent SDOF method. In this research, the equivalent SDOF method is also applied. Following is a SDOF based governing equation of a beam without damping as shown in Fig. 1

$$K_M M \ddot{x}(t) + K_L R(x) = K_L F_c(t) \tag{1}$$

or

$$K_{LM} M \ddot{x}(t) + R(x) = F_c(t) \tag{2}$$

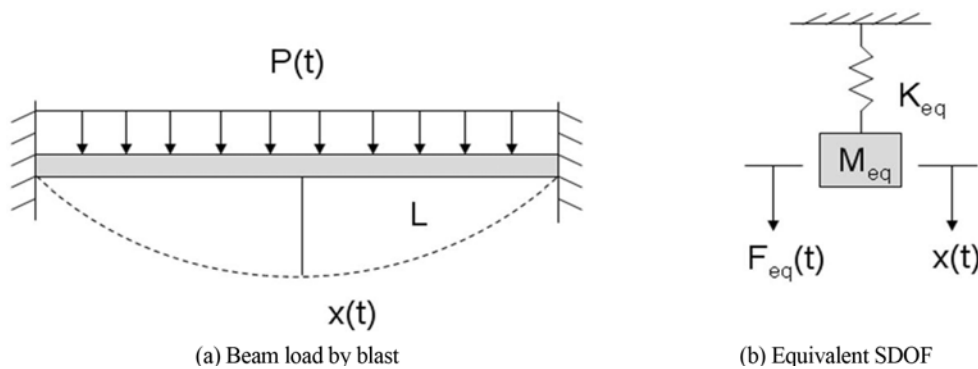


Fig. 1 Equivalent spring-mass SDOF system

where  $x$  is the midspan deflection,  $M$  is the total mass of the beam,  $R(x)$  is the resistance of the beam,  $F_c(t)$  is the applied force and equals to  $P(t)L$  as shown in Fig. 1,  $L$  is the span of the beam,  $K_M$  is mass factor of the beam,  $K_L$  is load factor of the beam, and  $K_{LM}$  is load-mass factor of the beam and equals to  $K_M/K_L$ .  $K_M$  and  $K_L$  are determined to have the same energy distribution and the work energy of the external load as that of the continuous beam responding in an assumed mode shape and can be computed as Eq. (3).

$$K_L = \frac{\int_0^L p(x)\varphi(x)dx}{\int_0^L p(x)dx}, \quad K_M = \frac{\int_0^L m(x)\varphi^2(x)dx}{\int_0^L m(x)dx} \tag{3}$$

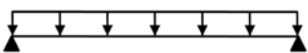
where  $p(x)$  is the dynamic load on blast-loaded component,  $\varphi(x)$  is the deflected shape function of the blast-loaded component,  $m(x)$  is mass per unit length of the blast-loaded component. Based on the assumed deflected shape  $K_M$  and  $K_L$  are shown in Table 1.

The resistance function ( $R-x$ ) of concrete structures under blast load is highly nonlinear. In this paper the function of structures is assumed to be elastic-perfectly plastic and tri-linear resistance functions for simple support beam and fixed support beam respectively and the slope of the unloading path is the same as that of loading path, as shown in Figs. 2(a) and (b).

The stiffness in the elastic domain and ultimate resistance which would cause a simple support beam yielding are shown as followings (TM 5-1300 1990)

$$K_e = \frac{384EI_e}{5L^3} \tag{4}$$

Table 1 Load, mass, and load-mass factors

Boundary Condition and Loading Diagram	Range of Behavior	Load Factor $K_L$	Mass Factor $K_M$	Load-Mass Factors $K_{LM}$
	Elastic	0.64	0.50	0.78
	Plastic	0.50	0.33	0.66

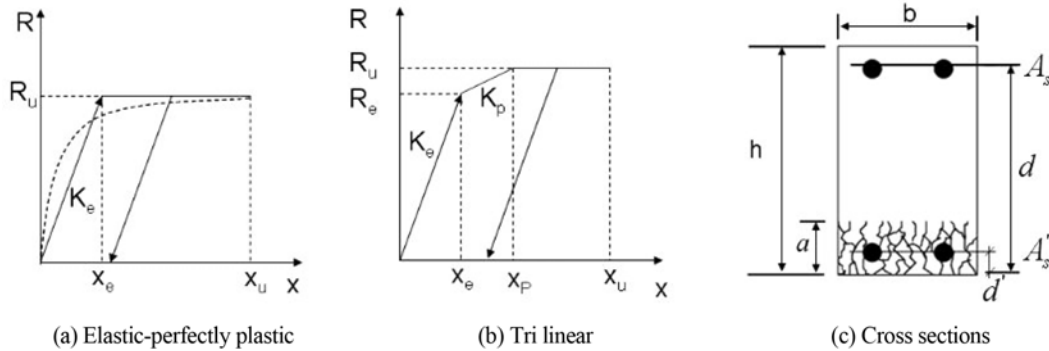


Fig. 2 Nonlinear resistance functions and their idealization of reinforced concrete beam

$$R_u = \frac{8M_u}{L} \tag{5}$$

where  $K_e$  is stiffness of the beam in elastic domain,  $L$  is the span of the beam,  $E$  is the elastic modulus of the concrete,  $I_e$  is the moment of inertia of the beam,  $R_u$  is ultimate resistance and  $M_u$  is the plastic moment capacity calculated based on the elastic range of behavior of reinforced concrete. In this paper  $M_u$  is computed as following (Krauthammer 2008)

$$M_u = A'_s f_{dy} (d - d') + (A_s - A'_s) f_{dy} (d - a/2) \tag{6}$$

in which

$$a = [(A_s - A'_s) f_{dy}] / 0.85 f'_c b \tag{7}$$

where  $a$  equals to depth of the concrete compression block,  $A_s$  and  $A'_s$  represent tensile and compressive reinforcement areas, respectively.  $b$  is the beam width,  $h$  is the total thickness/depth,  $d'$  is the distance from top compression face to center of the compression steel,  $d$  is the effective depth (distance from top fiber to center of tensile reinforcement),  $f_{dy}$  is the steel yield stress,  $f'_c$  is the concrete uniaxial strength. All above are shown in Fig. 2(c).

We have written a program with MATLAB software to solve the SDOF model numerically. The Newmark-beta method is adopted. The US Army uses the minimum value between 10% of the natural period and 3% of triangle positive loading duration as time step to solve an inelastic SDOF model (PDC-TR 06-01 Rev 1 2008). In this study, the time step was 0.1% of smallest value of natural periods and positive loading duration, which is compared to US Army approach.

The following steps are performed when the SDOF model is the main analysis tool used to assess a structural component under air blast loading(PDC-TR 06-01 Rev 1 2008):

- (1) The maximum allowable ductility ratio and support rotation are determined by protection level for the component types.
- (2) The airblast load is estimated considering the charge weight, standoff distance, and the angle between the explosion point and the normal plane of the member.
- (3) The maximum ductility ratio and support rotation of the member are calculated by using the SDOF method.
- (4) The calculated maximum ductility ratio and support rotation are compared to the predetermined maximum allowable ductility ratio and support rotation.
- (5) If the calculated response satisfies the allowable response, the member is safe. If not, the member is damaged.

Assuming symmetric load and deflection distributions, the support rotation is defined by the ratio of the calculated peak deflection to half a span length for one-way components

$$\tan \theta = \frac{2x_m}{L} \tag{8}$$

Acceptable maximum component damage levels are defined depending on the level of protection for each building and the component type in step (1). In this paper, the following damage ranges are used which are suggested in TM 5-1300 (1990):  $0^\circ \leq \theta \leq 2^\circ$ , light damage;  $2^\circ \leq \theta \leq 5^\circ$ , moderate damage;  $5^\circ \leq \theta \leq 12^\circ$ , severe damage.

### 3. Pressure-impulse diagrams

The pressure-impulse diagrams are used to relate the blast load to the corresponding damage where the flexural mode of failure dominates damage of the element. These diagrams incorporate both the magnitude and duration of blast loading to correlate blast load and corresponding damage which can be readily used for quick damage assessment of concrete structures under different blast scenarios. Fig. 3 shows primary features that define a P-I diagram. The two asymptotes, one for pressure and one for impulse, define limit values for each parameter. Loads with very short duration (relative to the structure's natural frequency) are called impulsive loading and the structure response is sensitive only to the associated impulse and not to the peak pressure. This forms a vertical line that defines the minimum impulse required to reach a particular level of damage, and the curve approaches asymptotically at high pressures. Conversely, as the load duration becomes longer than the natural frequency, the load is termed as quasi-static loading and the response becomes insensitive to impulse but very sensitive to peak pressure. The horizontal asymptote thus represents the minimum level of peak pressure required to reach that particular damage.

As can be seen, the pressure-impulse curve itself divides the pressure-impulse plane into two regions: the above and to the right of the curve where a damage level of the structure component is exceeded, and the below and to the left where the level is not exceeded. Pressure-impulse diagrams usually contain a group of pressure-impulse curves with different degrees of damage. These curves divide the pressure-impulse plane into several regions, each corresponding to a particular level of damage, and the curves themselves represent the boundaries between different damage levels, such as low damage, medium damage and high damage which has been prescribed in the last of Section 2 with different support rotations.

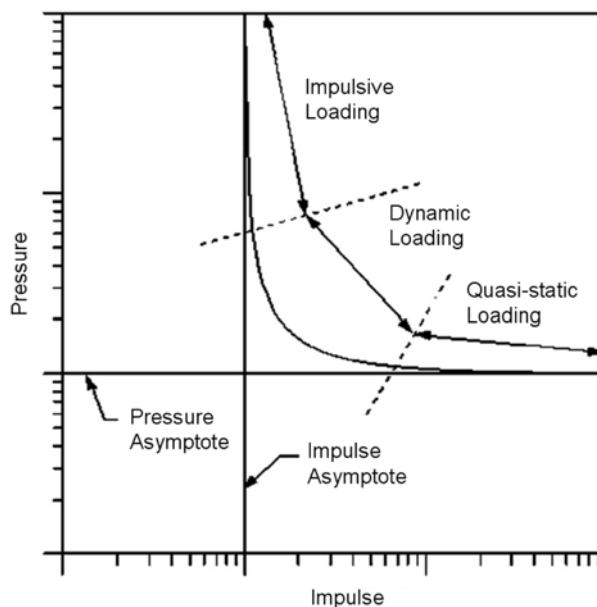


Fig. 3 Sketch of a typical pressure-impulse diagram

#### 4. Validation using experimental data

The fixed beam and one-way slab can be both analyzed in SDOF method under blast loading with the same boundary condition. The difference is that the width of slab is more than that of the beam and the height of slab is less than that of the beam. So the analysis procedure of slab is the same as beam which is prescribed in Section 2.

In this section a normal strength reinforced concrete slab has been used for developing resistance function and to obtain the pressure-impulse diagrams for different blast pressure impulse combinations. The slab, modeled here, was placed under open-air blast trial. Details of the slab and other test data can be found in Wu *et al.* (2009).

Dimensions of the slab are given in Fig. 4. These specimens were constructed with a 12 mm diameter mesh that was spaced in distance of 100 mm from each other in the major bending plane ( $\rho = 1.34\%$ ) and in distance of 200 mm from each other in the minor plane ( $\rho = 0.74\%$ ) where  $\rho$  is reinforcement ratio. The thickness of the concrete cover was 10 mm. The concrete had a cylinder compressive strength of 39.5 MPa, tensile strength of 8.2 MPa and Young's modulus of 28.3 GPa.

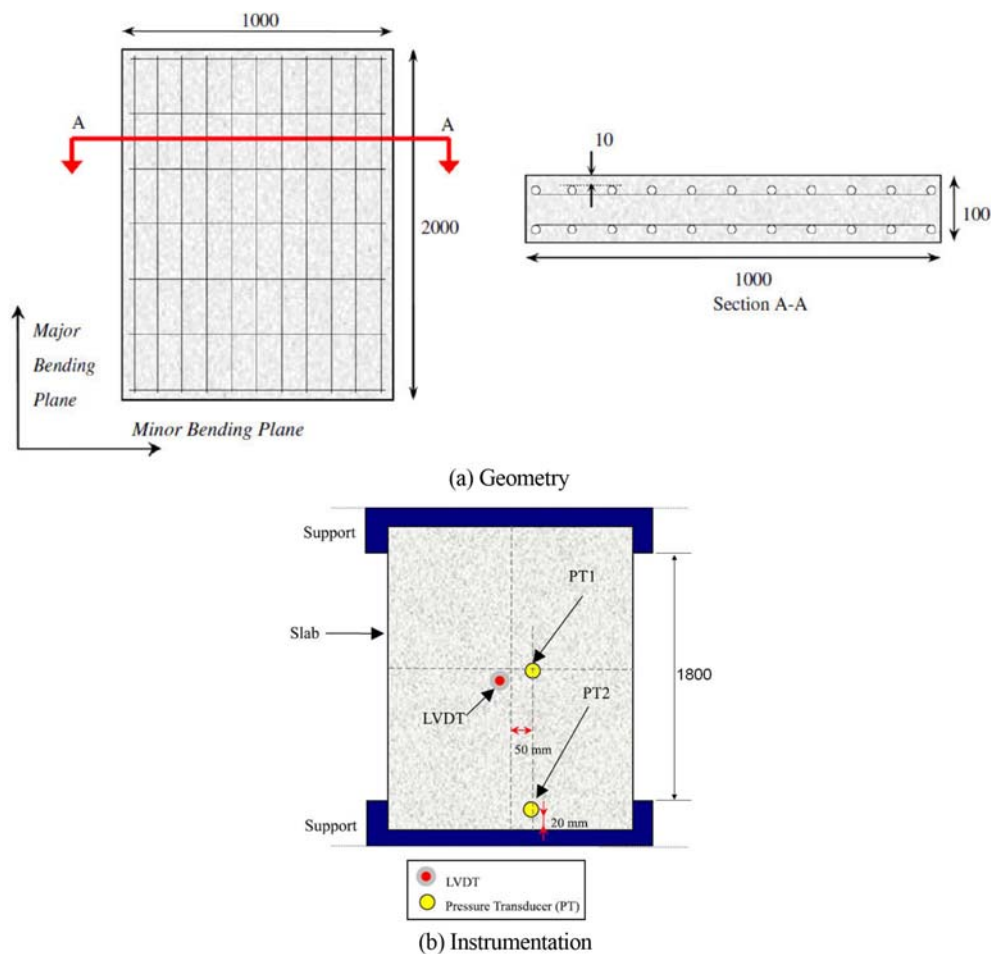


Fig. 4 Geometry of the RC slab (in mm) and instrumentation

Table 2 Experimental air blast program

Blast	Slab name	Dimension (mm)	Reinforcement ratio (%)	Standoff distance (m)	Scaled distance (m/kg <sup>1/3</sup> )	Explosive mass (g)
NRC-1	1A	2000 × 1000 × 100	1.34	3	3.0	1007
NRC-2	1A	2000 × 1000 × 100	1.34	3	1.5	8139
NRC-3	1B	2000 × 1000 × 100	1.34	1.4	0.93	3440
NRC-4	1A	2000 × 1000 × 100	1.34	1.5	0.75	8213
SLAB1	2	2500 × 500 × 150	1.34	/	/	/

Table 3 Experimental blast pressure summary

Blast	Slab name	Scaled distance to PT1 (m/kg <sup>1/3</sup> )	Peak reflected overpressure (MPa)		Reflected impulse (MPa·ms)	
			PT1	PT2	PT1	PT2
NRC-1	1A	3.0	0.42	0.30	0.186	0.133
NRC-2	1A	1.5	2.39	1.0	0.715	0.514
NRC-3	1B	0.93	6.38	1.49	0.705	0.638
NRC-4	1A	0.75	/	/	/	/

The reinforcement was of yield strength 600 MPa and Young's modulus 200 GPa.

The experimental test program is summarized in Table 2. The explosive charge was suspended above the center of the slab as described in Wu *et al.* (2009). As shown in Wu *et al.* (2009), negative pressure was negligible. The overpressure recorded at gauge PT1 was significantly larger than at PT2 in both specimens (refer to Fig. 4), indicating that the blast pressure on the slab was not uniform which was an expected result given the small standoff distance. A summary of the blast pressures recorded at PT1 and PT2 and the corresponding impulses are given in Table 3. Since the maximum pressure on the sensors was limited to 6.9 MPa, blast pressure history for NRC-4 was not recorded.

The end restraint in the test was somewhere between fixed and pinned, and the extent of fixity is likely dependent on the magnitude of the imposed blast load and the damage sustained by the restraints (Wu *et al.* 2009). If simple supports are assumed, the predicted maximum deflections of the tests are almost two times as the experiments of all four slabs. Thus the specimens are analyzed here assuming fixed supports. In the SDOF model, a tri-linear resistance-deflection curve as shown in Fig. 5 is used in analysis for fixed slab (PDC-TR 06-01 Rev 1 2008). For a SDOF system undergoing elastic deformation, yield resistance capacity  $R_e$ , ultimate resistance  $R_u$  of the cross-section, the stiffness  $K_e$  in the elastic domain and the stiffness  $K_p$  in the elastoplastic domain are given as follows

$$K_e = \frac{384EI}{L^3}, \quad K_p = \frac{384EI}{5L^3} \quad (9)$$

$$R_e = \frac{12M_u}{L}, \quad R_u = \frac{16M_u}{L} \quad (10)$$

where  $M_u$  is the yield moment which can be computed in Eq. (6) and  $L$  is the span.  $E$  is Young's

modulus and  $I$  is the average moment of inertia of the cross-section. The initial deflection and the final yield deflection can be calculated from

$$X_e = \frac{R_e}{K_e}, \quad X_p = X_e + K_p(R_u - R_e) \tag{11}$$

The ultimate deflection  $X_u$  in Fig. 5 is given by

$$X_u = \theta \frac{L}{2} \tag{12}$$

where  $\theta$  is the rotation angle derived by assuming that all of the rotation in the member take place over the plastic hinge length and curvature along the span is neglected.

From Wu *et al.* (2009), there is a slight lag between the arrival time at the mid-span and support and individual time-histories for the midspan and the support show instantaneous rise to peak pressure. The lag between the arrival time at the mid-span and support is very slight. So the pentagonal distributed load as shown in Fig. 6(a) is a better approximation of the actual blast load

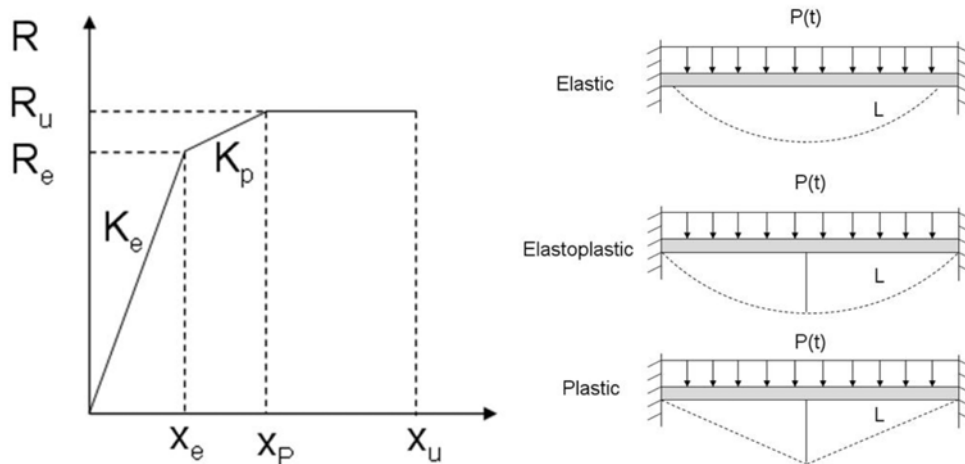


Fig. 5 Tri-linear resistance deflection curve and response modes of the slab

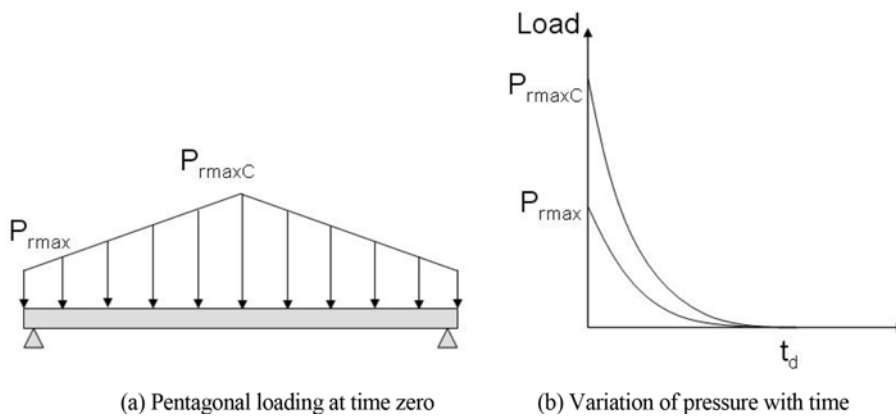


Fig. 6 Simplified pressure distributions

as shown in Jones *et al.* (2009). The total load on the entire slab surface is assumed instantaneously rise to peak load. It is an expected result given that the standoff distance and angle of incidence change as a function of location on the panel. Variables  $P_{r_{\max C}}$  and  $P_{r_{\max}}$  are the peak pressures at the center (PT1) and the edge (PT2) of the slab, respectively. The pressure time histories at the center and edge are simplified as exponential blast loads in Wu (2009) and Jones (2009) as shown in Fig. 6(b). The duration of the positive pressure wave  $t_d$  is back-calculated from the Eqs. (13) and (14).

$$P(t) = \begin{cases} P_{\max} \left[ 1 - \lambda \left( \frac{t}{t_d} \right) \right] e^{-\left( \frac{t}{t_d} \right)^\gamma}, & 0 < t < t_d \\ 0, & t > t_d \end{cases} \quad (13)$$

$$I = \int_0^{t_d} P(t) dt \quad (14)$$

where  $\gamma$  is shape constant of pressure waveform and equate to 2.8 and  $\lambda$  equate to 1 for exponential blast loads Li and Meng (2002a) in this paper. And  $P_{\max}$  in Eq. (13) in SDOF equals to  $P_{r_{\max C}}$  or  $P_{r_{\max}}$ , and  $I$  equals to  $I_1$  or  $I_2$  measured at the center (PT1) and the edge (PT2), when computed in SDOF1 model and SDOF2 model, respectively. Since the negative pressure phase does not affect significantly the maximum transient displacement of the slab as measured in the experiment (Wu *et al.* 2009) and should have only a small effect on the residual displacement, the negative phase is ignored in our computations.

The predicted maximum deflections of the tests using the SDOF1 model which the peak pressure is  $P_{r_{\max C}}$  and SDOF2 model which the peak pressure is  $P_{r_{\max}}$  in this paper are summarized in Table 4. The deflection of the SDOF1 model is higher than the measured maximum deflection and the deflection of the SDOF2 model is lower than the measured maximum deflection. The use of the SDOF1 model gives a very conservative prediction, partly because  $P_{r_{\max C}}$  is used as peak pressure of uniform loading of the equivalent SDOF load. The average deflection of the SDOF1 model and the SDOF2 model is compared well with the measured deflections, and the max prediction error is 17.1%.

Thus if the blast center is near the slab, the blast load is not uniform. The SDOF system can not capture the spatially and temporally varying distribution of the blast load. In order to modify the computed results, the blast should consider as pentagonal distributed load. And the results of the average computed results based on the overpressure history which is computed by empirical equation in both the centre and edge respectively are more accurate.

Table 4 Max deflection compared with experiments

Test	Max deflection (mm)				Prediction error (%)	
	Experiment	SDOF1	SDOF2	Average	SDOF1	Average SDOF
NRC-1	1.5	1.75	1.64	1.69	+17%	+13%
NRC-2	10.5	10.51	9.6	10.05	+0.1%	-4.2%
NRC-3	13.9	19.49	12.25	15.87	+18.7%	+14.1%
NRC-4	38.9	56.79	34.29	45.54	+40%	+17.1%

## 5. Slab damage and pressure-impulse diagram

In this section, a damage criterion shown in TM 5-1300 (1990) is prescribed first, and then the SODF solutions of three different load shapes with the same peak pressure and impulse combinations are compared. Based on the proposed damage criterion and SODF results, a pressure-impulse diagram generation method for a RC slab using SDOF and an analytical equation for the pressure-impulse diagram is proposed with different damage level and different blast load shapes.

### 5.1 Damage criterion

The deformation based damage criterion is used for the evaluation of local damage of a structural component subjected to blast loads in this paper. As shown in TM 5-1300 (1990) the following damage ranges are suggested:  $0^\circ \leq \theta \leq 2^\circ$ , Light damage;  $2^\circ \leq \theta \leq 5^\circ$ , Moderate damage;  $5^\circ \leq \theta \leq 12^\circ$ , Severe damage. So we define the damage Index as  $\theta = 2^\circ$ ,  $\theta = 5^\circ$  and  $\theta = 12^\circ$  as shown in Table 5.

In the study, the slab is 1800 mm long (with 200 mm long for supporting) as shown in Fig. 4. The different damage levels are shown in Table 5. And the damage index D can be defined as:  $\theta = 2^\circ$  when  $x_{\max} = 31.43$  mm;  $\theta = 5^\circ$  when  $x_{\max} = 78.74$  mm;  $\theta = 12^\circ$  when  $x_{\max} = 191.3$  mm where  $x_{\max}$  is the max displacement. This definition is subjective, but the physical meaning is clear.

### 5.2 SODF solutions with different load shapes

It is well known that the shape (or the time history) of a pressure pulse has a profound influence on the dynamic plastic response of structures when the pulse loading is represented by peak load and total impulse, which leads to difficulties to estimate the response and damage when a practical load cannot be described precisely as that can be shown in Li and Meng (2002a, b). However, the analysis in Li and Meng (2002a, b) is based on dimensional analysis and the influence of load shapes on the SDOF results has not been explored with the same peak pressure and impulse combination.

In this section, the blast load is defined as triangle, exponential and rectangular load shape respective to study the effect of blast load shape as shown in Fig. 7 on the structure response. The exponential load is defined as in Eq. (13). In order to compare the three blast loads effect, the loads are applied to the slab with the same peak pressure and impulse combination. From Fig. 7, one may notice that the loads are with the same peak pressure and impulse, but the load durations are different. The load duration of the rectangular load is the shortest, the triangle load duration is the second and is twice the duration of the rectangular load, and the exponential load has the longest

Table 5 Damage criterion of the slab

Damage level	Damage criterion of rotation	Damage criterion of displacement
Low damage	$0^\circ \leq \theta \leq 2^\circ$	$x_{\max} < 31.43$ mm
Medium damage	$2^\circ \leq \theta \leq 5^\circ$	$31.43$ mm $< x_{\max} < 78.74$ mm
High damage	$5^\circ \leq \theta \leq 12^\circ$	$78.74$ mm $< x_{\max} < 191.3$ mm
collapse	$12^\circ \leq \theta$	$x_{\max} > 191.3$ mm

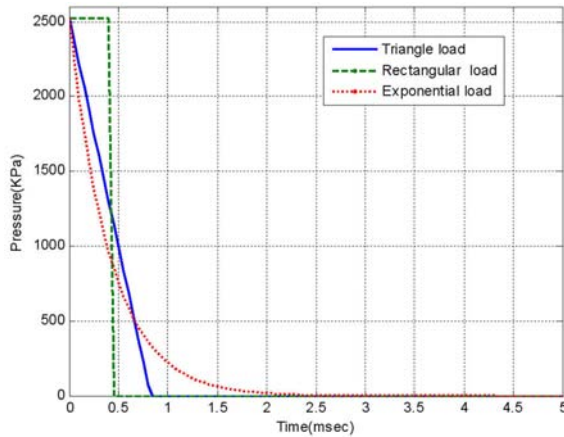


Fig. 7 Different load shapes

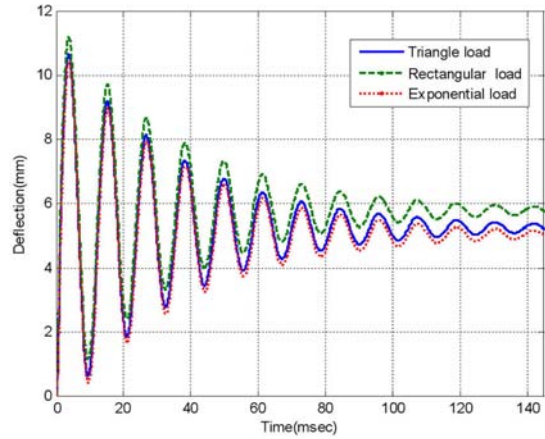


Fig. 8 Computed displacement history

load duration. But the high pressure duration is opposite; the rectangular load is the highest. Although the duration of the peak pressure of the triangular and the exponential loads are zero, the pressure in the triangular load is higher than the exponential load in the first 0.7 ms.

The response of the slab centre deflection is shown in Fig. 8. From the deflection caused by the three load shapes as shown in Fig. 8, the centre deflections of the slab are the same in the first several periods, and the periods of the three shapes of load are almost the same according to the same slab configurations. The difference of the deflections is that the peak deflection of the rectangle load is the highest and the exponential load is the lowest although the difference is small. For the peak load pressure exceeds the resistance of the slab there are plastic displacements for all the loads. The slab is suffered low damage as shown in Table 5 in these pressure pulses. But the residual deflections caused by the three loads are not the same, the rectangle load is the highest and the exponential load is the lowest.

It can be concluded that the damage level caused by blast is higher if the peak overpressure duration is longer with the same peak overpressure and impulse. So the pressure-impulse diagrams based on the maximal deflection of the slab are not the same with the same peak overpressure and impulse combination as discussed in the next section.

### 5.3 To generate pressure-impulse diagrams of different loads

Li and Meng (2002a, b) have studied the influence of the pulse shape on the P-I diagram for a linear-elastic SDOF system and an elastic-plastic SDOF system. But the influences of the pulse shape on the P-I diagram with different damage levels have not been studied. In this paper, different pressure impulse combinations have been applied to the slab to get the pressure-impulse points for both the near and far field condition using SDOF method. The blast loads are defined as triangle, exponential and rectangular load shape respective.

In this paper, a method was used to develop the P-I curves based on the written SDOF program. The P-I curves are based on 15 points where the blast load duration ranges from 0.05 to 60 times as shown in PDC-TR 06-01 Rev 1 (2008). The program is used to iterate on the peak pressure for each duration, calculating the maximum deflection for each trial peak pressure, until the maximum

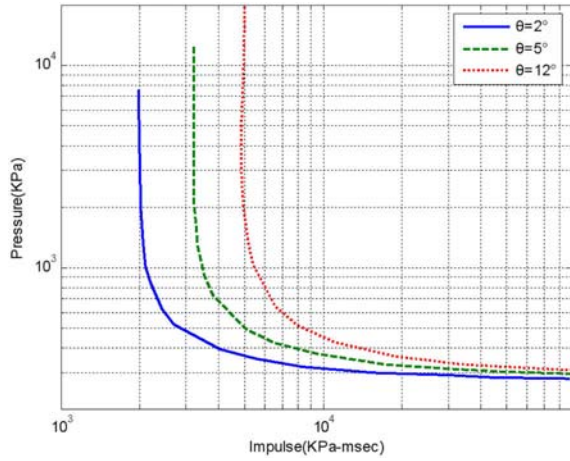


Fig. 9 Pressure-impulse diagram for the RC slab under triangle load (Interpolated curves)

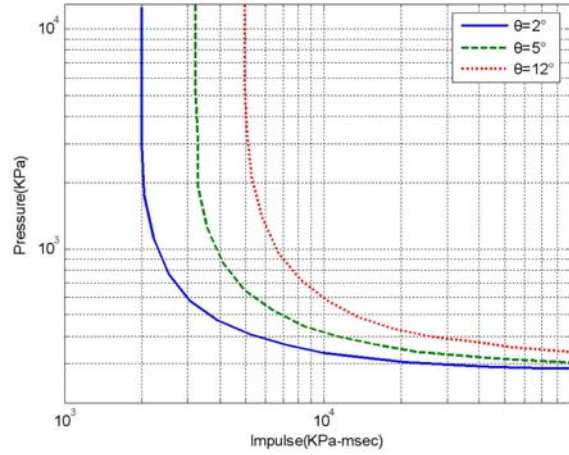


Fig. 10 Pressure-impulse diagram for the RC slab under exponential load (Interpolated curves)

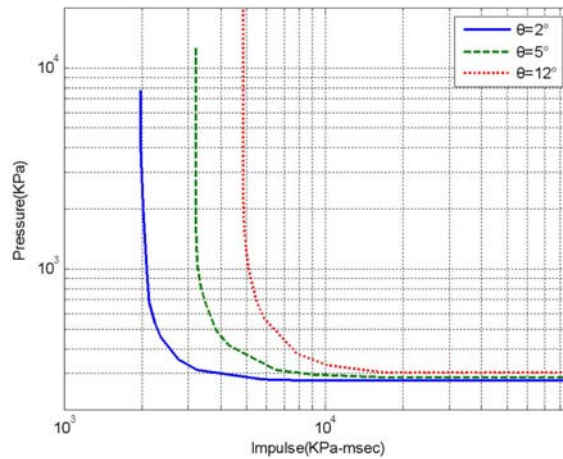


Fig. 11 Pressure-impulse diagram for the RC slab under rectangular load (Interpolated curves)

deflection for a given trial peak pressure equals the target maximum deflection within a small tolerance. After all the 15 points found, P-I curve can be plotted in the P-I diagram for each damage level as define before.

With different damage level as define before, the pressure-impulse diagrams are generated using SDOF with different blast load shape as shown in Figs. 9-11. As can be seen from these Figs, the pressure-impulse diagrams contain three pressure-impulse curves with different levels of damage  $\theta$ , they equal to  $2^\circ$ ,  $5^\circ$  and  $12^\circ$  respectively. These curves divide the pressure-impulse space into four regions, each corresponding to a particular level of damage. If the pressure impulse combination point is below and to the left of the curve  $\theta = 2^\circ$  the slab suffers low damage. And if the point is below and to the left of the curve  $\theta = 5^\circ$  but above and to the right of the curve  $\theta = 2^\circ$  the slab suffers medium damage. If the point is below and to the left of the curve  $\theta = 12^\circ$  but above and to the right of the curve  $\theta = 5^\circ$ , the slab suffers high damage. If the point is above and to the right of

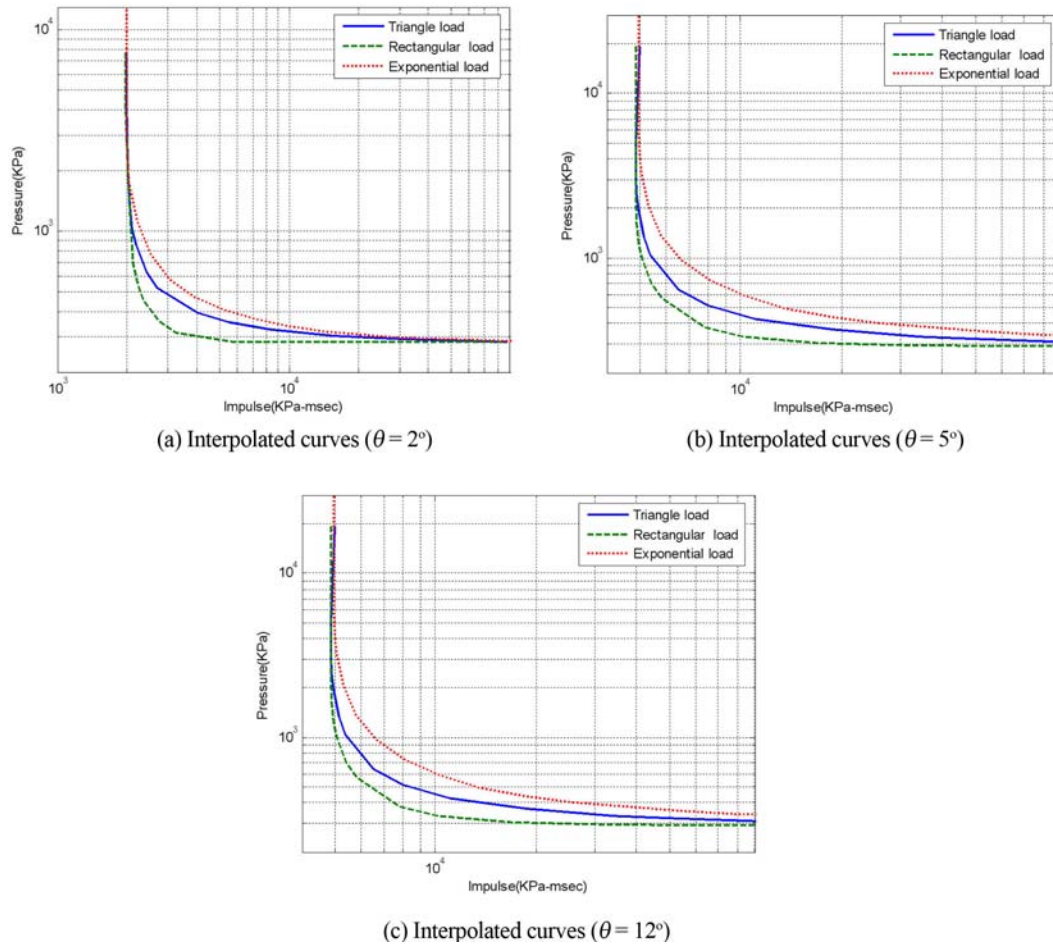


Fig. 12 Pressure impulse diagram of different damage level with three blast load shape

the curve  $\theta = 12^\circ$ , damage level of the slab is collapse.

The trends of the curves are the same in all three load shape pressure-impulse diagrams. The impulsive asymptotes of the curve the with different damage lever are evident in comparison with the quasi-static asymptotes. This is because, in the impulsive loading region, the blast load is usually of big peak and short duration, in such a short time, the flexural deflection needs more time to develop with respect different damage levels .

In order to compare different load shape's influence of the pressure-impulse diagrams, the pressure-impulse diagrams of the three loads with different damage level is shown in Fig. 12. It is found that the effects of pulse loading shape on the pressure-impulse diagrams are considerable. The load shape influences the pressure-impulse shape in the dynamic damage region for all three damage levels; the curves of rectangular load are the lowest in the diagrams and the curves of exponential load are the highest which is accordance with the SDOF results. The impulsive asymptote and the quasi-static asymptote are almost the same of the three blast load shapes with different damage level.

5.4 A simplified method to generate pressure-impulse diagrams of different loads

In this paper, a careful examination of the fitted pressure-impulse curves finds that they can be expressed analytically as

$$(P - P_\theta)(I - I_\theta)^n = 0.33 \left( \frac{P_\theta}{2} + \frac{I_\theta}{2} \right)^{1.5} \tag{15}$$

where  $n$  is the load shape factor,  $P_\theta$  is the pressure asymptote for damage degree  $\theta$ ,  $I_\theta$  is the impulsive asymptote for damage degree  $\theta$ . The  $P_\theta$  and  $I_\theta$  in Eq. (15) can be determined as follows: Perform SDOF method to obtain the damage degrees for the RC slab under blast loads in two ranges. One is in the impulsive loading range to get the value of  $I_\theta$ , and the other is in the quasi-static loading range to get the value of  $P_\theta$ . The best fitted pressure-impulse curves according to Eq. (15) are plotted in Figs. 13-16. When the blast load is simplified as exponential, triangle, and rectangular load,  $n$  equals to 0.6, 0.7 and 0.8 respectively. It shows that the pressure-impulse curves almost fit different damage levels. This demonstrates that Eq. (15) can be used to model pressure-impulse curves for the slabs with different damage levels and different load shapes.

Further study is conducted to investigate whether Eq. (15) can be used for other one-way RC slabs. The same procedure is used to estimate damage degrees of RC slab1 under different blast loads. The configuration of slab1 is also given in Table 2. The concrete strength and the reinforcement ratio is the same with the NRC slab. The damage levels with respect to peak pressure and impulse of the three blast load sharps are plotted in the pressure-impulse space in Figs. 17-19. The best-fitted pressure-impulse curves according to Eq. (15) are also plotted in Figs. 17-19. It shows that the pressure-impulse curves almost fit the boundary lines between different damage curves and blast load sharps. This demonstrates that Eq. (15) can be used to model pressure-impulse curves for all RC slabs.

In this paper the asymptotes of the pressure-impulse diagrams of NRC1 and slab1 is shown in Table 6 and Table 7. It can be concluded from Table 6 and Table 7 that the exponential blast load has the highest pressure asymptote  $P_\theta$  and impulsive asymptote  $I_\theta$  according to different damage

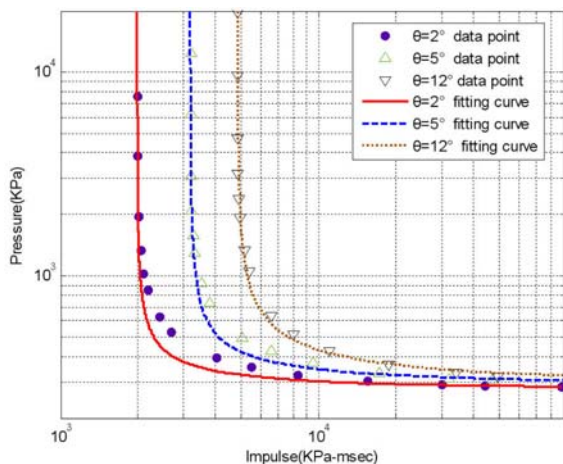


Fig. 13 Pressure-impulse diagram for the RC slab under triangle load (Fitting curves)

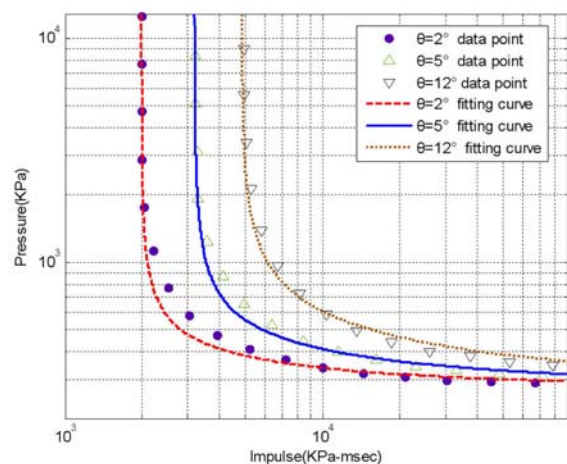


Fig. 14 Pressure-impulse diagram for the RC slab under exponential load (Fitting curves)

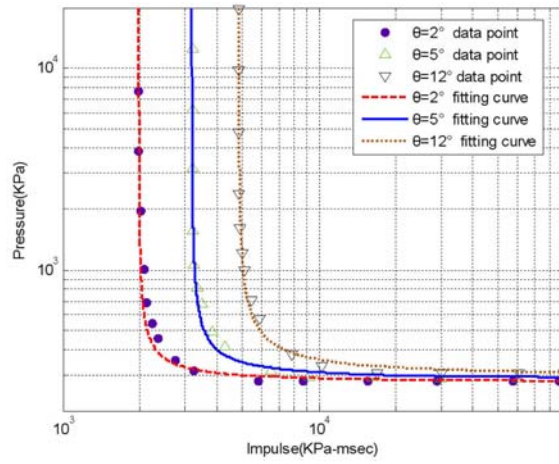


Fig. 15 Pressure-impulse diagram for the RC slab under rectangular load (Fitting curves)

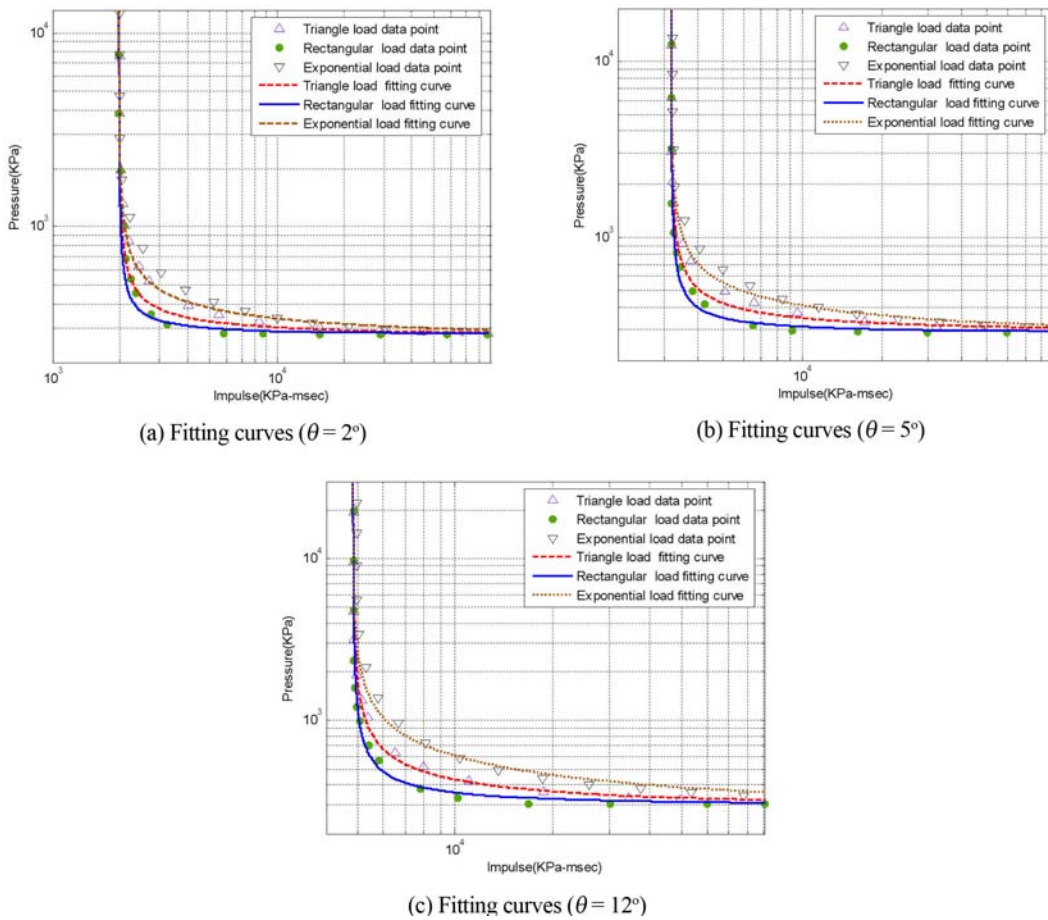


Fig. 16 Pressure impulse diagram of different damage level with three blast load shape

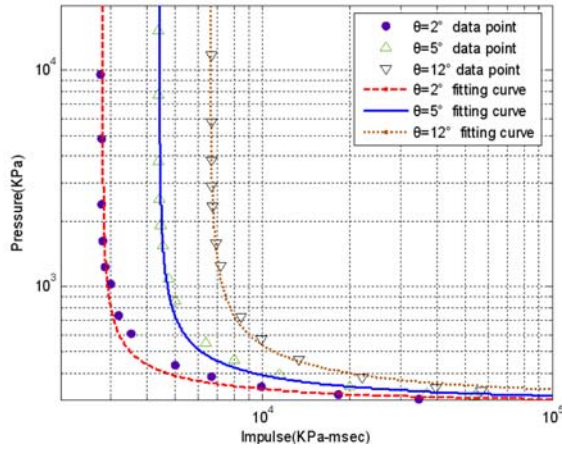


Fig. 17 Pressure-impulse diagram for the RC slab1 under triangle load (Fitting curves)

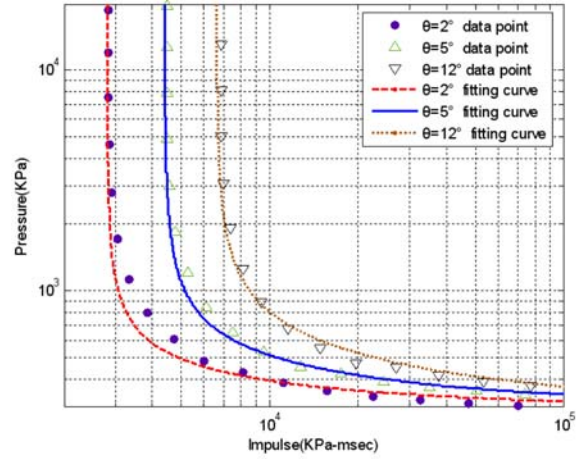


Fig. 18 Pressure-impulse diagram for the RC slab1 under exponential load (Fitting curves)

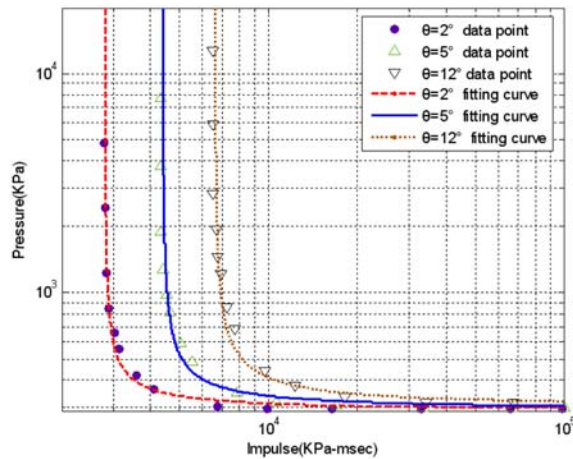


Fig. 19 Pressure-impulse diagram for the RC slab1 under rectangular load (Fitting curves)

Table 6 Pressure asymptote  $P_\theta$  (KPa) and impulsive asymptote  $I_\theta$  (KPa-ms) for NRC slab

Load shape	$P_{2^\circ}$	$I_{2^\circ}$	$P_{5^\circ}$	$I_{5^\circ}$	$P_{12^\circ}$	$I_{12^\circ}$
Triangle	282.73	1984.4	298.14	3198.4	308.64	4859.1
Exponential	284.58	1984.5	303.86	3216.1	310.48	4973.2
Rectangular	279.63	1981.3	289.09	3203.6	305.53	4859.6

Table 7 Pressure asymptote  $P_\theta$  (KPa) and impulsive asymptote  $I_\theta$  (KPa-ms) for slab1

Load shape	$P_{2^\circ}$	$I_{2^\circ}$	$P_{5^\circ}$	$I_{5^\circ}$	$P_{12^\circ}$	$I_{12^\circ}$
Triangle	298.5	2746	306.54	4424.8	312.16	6632.7
Exponential	297.99	2829.8	307.46	4461.8	317.33	6817.7
Rectangular	293.91	2755.3	299.7	4332.9	311.98	6508.6

level and the rectangular blast load is the least of the two asymptotes. But the difference is very small. In fact the blast load is exponential load shape for most cases, when the blast load is simple as triangle blast load, the pressure-impulse diagrams has lower damage assessment and the prediction is conservative.

According to the previous discussions, the procedure to generate a pressure-impulse diagram for a RC slab can be simplified to the following two steps:

- (1) Perform SDOF method to obtain the damage degrees for the RC slab under blast loads in two ranges. One is in the impulsive loading range to get the value of  $I_{\theta}$ , and the other is in the quasi-static loading range to get the value of  $P_{\theta}$ . The results (damage level) together with the pressure asymptote and impulse asymptote are then plotted in the pressure-impulse space as shown in Table 6.
- (2) Using Eq. (15) as the regression model, obtain the best fitted pressure-impulse curves, which are the boundaries of different damage levels.

## 6. Conclusions

In this paper, a modified method of obtaining pressure-impulse diagrams of one-way reinforced concrete slab is developed by using SDOF model. It is shown the SDOF method and pressure-impulse diagrams can be used to assess damage of slabs subjected to blast loading and is validated using published test data.

For close-in explosions blast load is not uniform spatially, and the SDOF can not capture a spatially and temporally varying distribution of the blast load. The results of the average computed SDOF results based on the overpressure history are more accurate in both the centre and edge respectively.

A SDOF analysis can give a preliminary assessment for a protective structure. The proposed method can be applied from a single structural element to an integrated structural frame. It is found that the effects of pulse loading shape on the pressure-impulse diagrams are considerable. The blast load shape influences the pressure-impulse shape in the dynamic damage region for all three damage levels; the curves of rectangular load are the lowest in the diagrams and the curves of exponential load are the highest, which are accordance with the SDOF results. The impulsive asymptote and the quasi-static asymptote are almost the same for the three blast load shapes with different damage index. It is shown that if the blast load is simple as triangle blast load, the pressure-impulse diagrams has lower damage assessment and the prediction is conservative. Based on the results of the derived pressure-impulse diagrams, an analytical equation for the pressure-impulse diagram for RC slabs is proposed.

## References

- Army TM 5-1300 (1990), "Structures to resist the effects of accidental explosions", US Department of the Army.
- Army TM 5-855-1 (1986), "Fundamentals of protective design for conventional weapons", US Department of the Army.
- Bangash, M.Y.H. (1993), "Impact and explosion-analysis and design", Oxford: Blackwell Scientific Publication.

- Baker, W.E., Cox, P.A., Westine, P.S., Kulesz, J.J. and Strehlow, R.A. (1983), *Explosion hazards and evaluation*, Amsterdam, Elsevier Scientific Pub. Co., New York.
- Biggs, J.M. (1964), *Introduction to Structural Dynamics*, McGraw-Hill.
- Fallah, A.S. and Louca, L.A. (2007), "Pressure-impulse diagrams for elastic-plastic-hardening and softening single-degree-of-freedom models subjected to blast loading", *Int. J. Impact Eng.*, **34**, 823-842.
- Kappos, A.J. (2002), *Dynamic Loading and Design of Structures*, Spon Press, London.
- Jones, J., Wu, C., Oehlers, D.J., Whittaker, A.S., Sun, W., Marksa, S. and Coppola, R. (2009), "Finite difference analysis of simply supported RC slabs for blast loadings", *Eng. Struct.*, **31**, 2825-2832.
- Krauthammer, T., Astarlioglu, S., Blasko, J., Soh, T.B. and Ng, P.H. (2008), "Pressure-impulse diagrams for the behavior assessment of structural components", *Int. J. Impact Eng.*, **35**, 771-783.
- Krauthammer, T. (2008), *Modern Protective Structures*, CRC Press.
- Lan, S.R. and Crawford, J.C. (2003), "Evaluation of the blast resistance of metal deck proofs", *Proceeding of the Fifth Asia-pacific Conference on Shock & Impact Loads on Structures*, Changsha, Hunan, China.
- Li, Q.M. and Shu, X.F. (1992), "Elimination of loading shape effects on blast loading beams in damping medium", *Proceedings of the International Symposium on Intense Dynamic Loading and Its Effects*, Chengdu.
- Li, Q.M. and Jones, N. (1994), "Blast loading of fully clamped circular plates with transverse shear effects", *Int. J. Solids Struct.*, **31**, 1861-1876.
- Li, Q.M. and Jones, N. (1995a), "Blast loading of fully clamped beams with transverse shear effects", *Mech. Struct. Mach.*, **23**, 59-86.
- Li, Q.M. and Jones, N. (1995b), "Blast loading of a "short" cylindrical shell with transverse shear effects", *Int. J. Impact Eng.*, **16**, 331-353.
- Li, Q.M. and Jones, N. (2001), "Foundation of correlation parameters for eliminating pulse shape effects on dynamic plastic response of structures", Impact Research Center Report, Department of Mechanical Engineering, University of Liverpool.
- Li, Q.M. and Meng, H. (2002a), "Pressure-impulse diagram for blast loads based on dimensional analysis and single-degree-of-freedom model", *J. Eng. Mech.-ASCE*, **128**(1), 87-92.
- Li, Q.M. and Meng, H. (2002b), "Pulse loading shape effects on pressure-impulse diagram of an elastic-plastic, single-degree-of-freedom structural model", *Int. J. Mech. Sci.*, **44**, 1985-1998.
- Ma, G.W., Shi, H.J. and Shu, D.W. (2007), "P-i diagram method for combined failure modes of rigid-plastic beams", *Int. J. Impact Eng.*, **34**, 1081-1094.
- Mays, G.C. and Smith, P.D. (1995), *Blast Effects on Buildings-design of Buildings to Optimize Resistance to Blast Loading*, Thomas Telford, London.
- Park, J.Y. and Krauthammer, T. (2009), "Inelastic two-degree-of-freedom model for roof frame under airblast loading", *Struct. Eng. Mech.*, **32**, 321-335.
- PDC-TR 06-01 Rev 1 (2008), "Methodology manual for the Single degree of freedom blast effects design spreadsheets", US Army Corps of Engineers.
- Shi, Y.C., Hao, H. and Li, Z.X. (2008), "Numerical derivation of pressure-impulse diagrams for prediction of RC column damage to blast loads", *Int. J. Impact Eng.*, **35**, 1213-1227.
- Smith, P.D. and Hetherington, J.G. (1994), "Blast and ballistic loading of structures", Butterworth-Heinemann, Oxford, 1-336.
- Symonds, P.S. (1953), "Dynamic load characteristics in plastic bending of beams", *ASME J. Appl. Mech.*, **20**, 475-81.
- Wesevich, J.W. and Oswald, C.J. (2005), "Empirical based concrete masonry pressure-impulse diagrams for varying degrees of damage", *Proceedings of the 2005 Structures Congress and the 2005 Forensic Engineering Symposium*, New York.
- Wu, C., Oehlers, D.J., Rebentrost, M., Burman, N. and Whittaker, A.S. (2009), "Blast testing of ultrahigh performance fiber concrete slabs and FRP retrofitted RC slabs", *Eng. Struct.*, **31**, 2060-2069.
- Youngdahl, C.K. (1970), "Correlation parameters for eliminating the effect of pulse shape on dynamic plastic deformation", *ASME, J. Appl. Mech.*, **37**, 744-752.
- Zhu, G., Huang, Y.G., Yu, T.X. and Wang, R. (1986), "Estimation of the plastic structural response under impact", *Int. J. Impact Eng.*, **4**, 271-282.